Counting Elementary Charges on Nanoparticles by Electron Holography

C. Gatel,[1,*] A. Lubk,[1,2] G. Pozzi,[3] E. Snoeck,[1] and M. Hÿtch[1]

[1]*CEMES-CNRS and Université de Toulouse, 29 rue Jeanne Marvig, 31055 Toulouse, France*
[2]*Institute of Structure Physics, Technische Universität Dresden, 01062 Dresden, Germany*
[3]*Department of Physics and Astronomy, University of Bologna, Viale Berti Pichat 6/2, 40127 Bologna, Italy*

(Received 24 July 2012; revised manuscript received 22 April 2013; published 10 July 2013)

The distribution and movement of charge is fundamental to many physical phenomena, particularly for applications involving nanoparticles, nanostructures, and electronic devices. However, there are very few ways of quantifying charge at the necessary length scale. Here, we show that aberration-corrected electron holography is capable of counting the charge on individual nanoparticles to a precision of one elementary unit of charge. We present a method that measures charges within predefined contours by directly applying Gauss's law at the nanoscale. We perform a statistical analysis to reveal the relationship between the size of the contours and the precision of the charge measurement and present strategies to optimize the spatial and signal resolution for the presented method.

DOI: 10.1103/PhysRevLett.111.025501 PACS numbers: 61.05.jp, 07.05.Pj, 84.37.+q

Introduction.—A number of scanning probe microscopy (SPM) techniques have been developed to detect and even manipulate single electrons at the nanoscale, i.e., single-electron transistor scanning electrometer (SETSE) [1], scanned capacitance microscopy [2], charge sensing by atomic force microscopy (AFM) [3], or single-electron electrostatic force microscopy (*e*-EFM) [4,5]. Static electric fields and charges with 100-nanometer spatial resolution and a charge sensitivity of a small fraction of an electron can be achieved by SETSE [1]. The electrostatic force resulting from single electrons tunneling into and out of quantum dots can be detected by AFM or *e*-EFM [3,5]. However, SPM techniques also suffer from drawbacks: measurements are optimized for particular electrical boundary conditions (e.g., conducting objects on insulating surfaces for AFM) and ultrahigh vacuum conditions, the measured forces and currents are highly nonlinear with respect to the charge state and scanning the specimen introduces artifacts such as distortions.

Transmission electron microscopy (TEM) [6], and, in particular, off-axis electron holography (EH) [7–9], has long been used to study charges and charge distributions on nanoparticles and nanostructures. The technique has notably less sensitivity than SPM and one must consider that the electron beam can locally modify the initial charge distribution [10,11]. However, EH has the advantage that the phase measured in the electron hologram is linearly related to the electrostatic potential experienced by the fast electron and can be used to quantify electrostatic fields, for example, in doped regions of transistors [12,13]. Furthermore, the effect of electron-beam induced charging plays an important role for investigating a wide range of materials in TEM, e.g., semiconductors [10,14–17]; i.e., an accurate electron holographical characterization of beam induced charges itself is highly beneficial.

In general, previous EH measurements were based on fitting models for the electrostatic potential to the EH phase. Such indirect methods suffer from the usual limitations that *a priori* knowledge is required to construct the models. Charge distributions need to be postulated beyond the field of view because their long-range electrostatic fields may modify the reference wave required within the EH experimental setup (see Fig. 1) [18,19]. The measurement is therefore nonunique. Nevertheless, a charge of about 100 electron charges (q_e) was recently quantified in the well-defined system of isolated latex spheres [20].

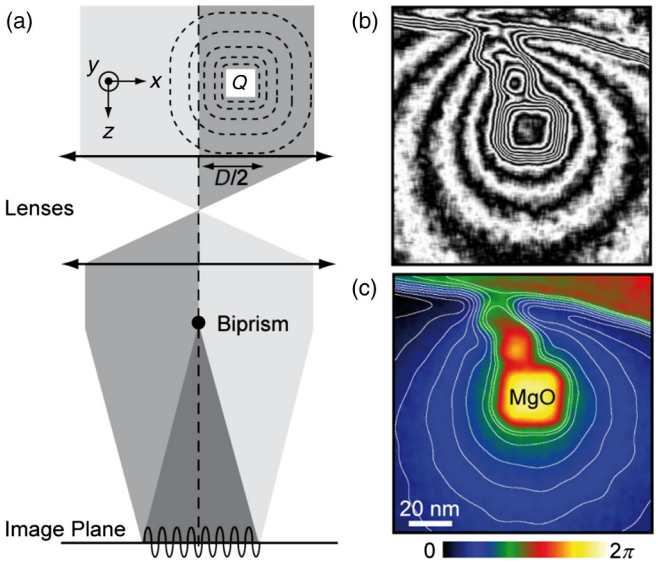

FIG. 1 (color online). Observing charge on nanoparticles. (a) Holographic setup, (b) amplified cosinus contour map (13 ×) of the reconstructed phase of a charged MgO particle and (c) false color representation of the reconstructed phase with contours (every 0.3 rad).

Here, we present a direct method of measuring charge from electron holograms that overcomes these problems. The method follows the work of Beleggia *et al.* [21] and is based on applying Gauss's Law at the nanoscale. In combination with state-of-the-art off-axis aberration-corrected electron holography we demonstrate the possibility of directly measuring, for isolated nanoparticles, their total charge with a unprecedented precision of about one elementary charge ($\sim 1q_e$).

Theoretical basis.—The basic geometry of off-axis EH applied to electrostatic fields is illustrated in Fig. 1(a). We will denote 3D vectors by $\mathbf{r} = (x, y, z)^T$ and 2D vectors in the object (and conjugated) xy planes by $\mathbf{R} = (x, y)^T$ in the following. Two coherent electron waves $\psi_{l,r}(\mathbf{R}) = A_{l,r}(\mathbf{R})\exp(i\phi_{l,r}(\mathbf{R}))$ passing on the left and right side of a filament (biprism) can be made to overlap by applying a suitable voltage to the biprism, thereby creating a sinusoidal interference pattern with spatial wave vector $\mathbf{K}_0$ [22]:

$$I(\mathbf{R}) = |A_l(\mathbf{R})|^2 + |A_r(\mathbf{R})|^2 + 2A_l(\mathbf{R})A_r(\mathbf{R})\cos(\mathbf{K}_0 \cdot \mathbf{R} + \phi_l(\mathbf{R}) - \phi_r(\mathbf{R})). \quad (1)$$

The phase difference between the two beams $\phi(\mathbf{R}) = \phi_l(\mathbf{R}) - \phi_r(\mathbf{R})$ is then extracted by Fourier filtering (see below). Within the phase object approximation [18,19,23], which is valid for the slowly varying or weak electrostatic potentials investigated here, the phase of the reconstructed wave is proportional to the specimen potential integrated along the incident beam direction:

$$\varphi(\mathbf{R}) = C_E \int \left(V\left(\mathbf{r} + \frac{\mathbf{d}}{2}\right) - V\left(\mathbf{r} - \frac{\mathbf{d}}{2}\right)\right) dz, \quad (2)$$

where C_E is a constant that only depends on the electron energy and universal constants ($C_E = 0.0073$ rad$/(V \cdot$ nm) for an accelerating voltage of 200 keV) and $\mathbf{d} = (\mathbf{D}, 0)^T$ denotes the lateral shift between the two wave fronts (see Fig. 1). Here and in the following, we can safely neglect magnetic contributions because they do not contribute to the following charge determination based on Gauss law (div$\mathbf{B} = 0$). They can be, however, revealed by a different integration scheme [24].

According to the superposition principle we can now separate the electrostatic potential and the resulting phase into two parts: one stemming from the neutral crystal denoted by "cr" (which corresponds to the mean inner potential—MIP [25]), and the other arising solely from additional charges denoted by Q:

$$\phi(\mathbf{R}) = \phi_{\mathrm{cr}}(\mathbf{R}) + \phi_Q(\mathbf{R}). \quad (3)$$

First, let us analyze the phase image of the charge, putting to aside for the moment the MIP contribution. The total charge Q within a chosen region can be uniquely retrieved by integrating the 2D Laplace operator applied to the phase provided that the reference region does not contain any charges ($\iiint \rho(\mathbf{r} - (\mathbf{d}/2))d^3r = 0$):

$$\begin{aligned}\iint \Delta_R\varphi_Q(\mathbf{R})d^2R &\overset{\text{Eq. (2)}}{=} C_E \iiint \Delta_R\left(V_Q\left(\mathbf{r} + \frac{\mathbf{d}}{2}\right) - V_Q\left(\mathbf{r} - \frac{\mathbf{d}}{2}\right)\right)d^3r \\ &\overset{\lim_{z\to\infty} E_z(\mathbf{r})=0}{=} C_E \iiint \Delta\left(V_Q\left(\mathbf{r} + \frac{\mathbf{d}}{2}\right) - V_Q\left(\mathbf{r} - \frac{\mathbf{d}}{2}\right)\right)d^3r \\ &\overset{\text{Gauss's law}}{=} -\frac{C_E}{\varepsilon_0}\iiint \rho\left(\mathbf{r} + \frac{\mathbf{d}}{2}\right)d^3r \\ &= -\frac{C_E}{\varepsilon_0}Q. \end{aligned} \quad (4)$$

Here, the crucial point was adding ∂^2V/∂^2z on the second line, which integrates to zero if the electric field in the z direction vanishes at infinity because $\int(\partial^2V/\partial^2z) = E_Z|_{-\infty}^{\infty}$. As a further refinement, we use the equivalence with a contour integral (line parameter s, outward normal $\mathbf{N}$) in two dimensions:

$$\iint \Delta_R\varphi_Q(\mathbf{R})d^2R = \oint_C \nabla_R\varphi_Q(\mathbf{R}(s)) \cdot \mathbf{N}(\mathbf{R}(s))ds, \quad (5)$$

to obtain a more suitable relationship for the charge

$$Q = -\frac{\varepsilon_0}{C_E}\oint_C \nabla_R\varphi_Q(\mathbf{R}(s)) \cdot \mathbf{N}(\mathbf{R}(s))ds, \quad (6)$$

which suppresses problems arising from singularities appearing in phase derivatives close to charge centers and uses only a simple phase gradient. The power of Gauss's law is that the result is independent of any particularly contour C, and therefore by choosing suitable contours enclosing the region of interest, it is possible to obtain several values for the enclosed charge, whose statistical processing allows for a significant reduction of errors and an estimation of the precision. Furthermore, the method provides direct access to the total charge enclosed by a given contour without assuming further details about neither the position of the charges within or outside the field of view nor the material investigated, contrary to a model-based approach where the whole electrostatic potential has to be computed. The reduction of the estimated parameter space improves the precision and accuracy of the obtained charge.

Equation (6) constitutes the basis of our measurement scheme which we will develop after discussing possible deviations and artifacts. We first note that the presence of additional electric fields, or linear phase ramps introduced by the reconstruction process or from disturbances in the reference wave [19], will not disturb the charge that is measured. Neither is the method affected by residual high frequency aberrations (see Supplemental Material [26], Suppl. B) if the measured charge is spread over distances large compared to the spatial resolution of the holographic reconstruction. (5 nm in our case, a detailed derivation of that statement is given in the Supplemental Material [26], Suppl. B). The main limitation is currently imposed by the limited signal resolution of the

reconstructed phase and the impact of the potential of the crystal lattice, which will be discussed next.

Because of the strong interaction of the electron beam with atomic potentials inhomogeneities in crystal structures, such as defects, bending, or phase boundaries can lead to strong reconstructed phase gradients, in particular under low-index zone axis conditions (dynamic scattering). Even in the case of a sufficiently homogeneous structure, where V_{cr} is uniform within the material and equal to the mean inner potential [27], the phase image

$$\varphi_{\mathrm{cr}}(\mathbf{R}) = C_E \int_0^{t(\mathbf{R})} V_{\mathrm{cr}}(\mathbf{r}) dz \approx C_E V_{\mathrm{cr}} t(\mathbf{R})$$

varies with thickness $t(\mathbf{R})$ and all such noncharge related variations can severely hamper the evaluation of contour integrals *within* the particles. Here, we adopted three different strategies to suppress their influence when measuring inside particles: First, the MgO cubes analyzed were oriented into ⟨100⟩-direction with negligible thickness variations, second, we deliberately chose contours that locally are parallel to $\nabla_{\mathrm{R}} t(\mathbf{R})$ at the particle edges, and third, very large phase gradients not originating from charges have been suppressed (details are discussed below and in the Supplemental Material [26], Suppl. B and C).

Methods.—Nanocuboids of MgO of a large variety of sizes (5–200 nm) have been synthesized by simply burning pure Mg foil and intercepting the resulting MgO smoke on a lacey carbon grid [28]. These insulating MgO nanocubes are electrically charged, or become so under the electron beam by knockout of secondary electrons. Because of their well-defined geometry, low-scattering power and large variety of sizes, these nanocuboids can be considered as model nano-objects for the study of the electron charge density. In order to suppress thickness gradients within the cube, only ⟨100⟩-oriented cuboids have been considered.

Holograms of MgO nanocuboids were digitally acquired using a FEI Tecnai-F20 microscope (200 kV) fitted with a spherical aberration Cs-corrector (CEOS) in a Lorentz Cs-corrected mode. Holographic reconstruction was performed with the help of Holodark 1.0 (HREM Research Inc.) a plug-in for Digital Micrograph™ (Gatan). The phase images were obtained by reconstructing the aberration-corrected holograms using the Fourier method, where one of the interference terms (side band) is isolated by applying a low-pass filter which defines the resulting phase image resolution of 5 nm in our case corresponding approximately to the resolution of our Lorentz lens.

A dedicated Digital Micrograph software plug-in has been developed for performing the charge evaluation based on line integration (see the Supplemental Material [26], Suppl. C). Following Eq. (6), we employed a set of contour integrals with increasing size as illustrated in Fig. 2 (see the Supplemental Material [26], Suppl. C). The rectangular contours are aligned with respect to the cube edges, crossing them at 90° in such a way as to minimize the influence

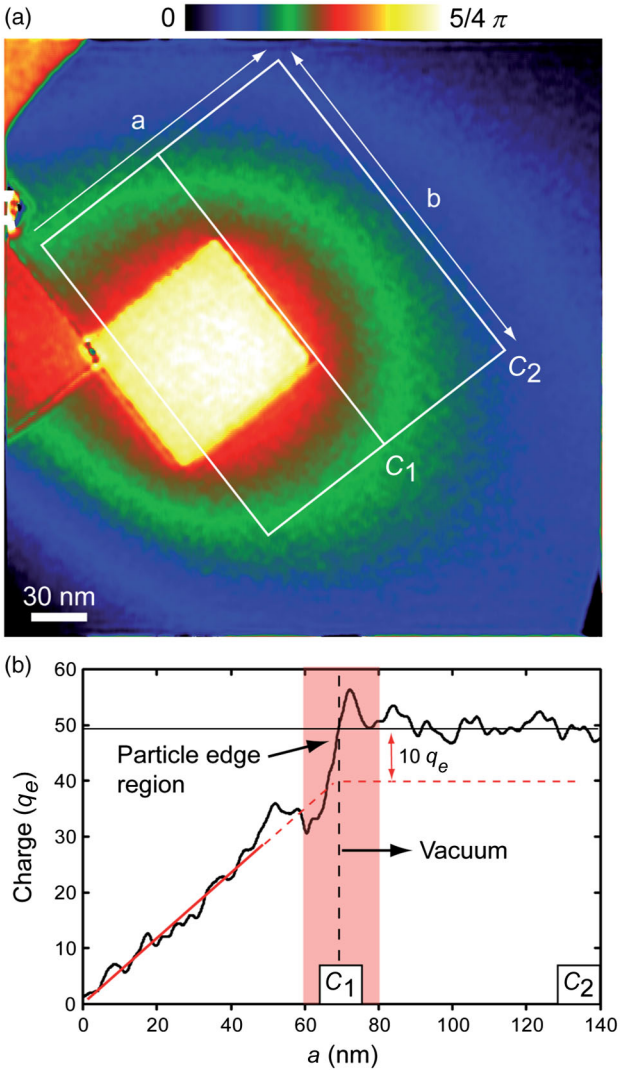

FIG. 2 (color online). Charge measurements. (a) Reconstructed phase image of particle 1, (b) by contour enclosed charge as a function of the short side a; the linear fit of contours within the particle and the constant fit outside of the particle are indicated by red and black lines, respectively.

of thickness gradients at the particle edges. To further suppress both the influence of artificially large phase gradients at thickness discontinuities and possible reconstruction artifacts, we additionally applied a threshold filter to remove a very small number ($< 5\%$) of excessive gradients from the line integration (see the Supplemental Material [26], Suppl. C).

Results.—We first report on the charge measurements in a $75 \times 78 \times 80$ nm MgO cuboid [Fig. 2(a), see the Supplemental Material [26], Suppl. A for dimension measurement], which is located on top of another cube, assuring its electrical insulation from the carbon support. Multiple rectangular contour integrals presented in the Supplemental Material [26], Suppl. C, all sharing one side as illustrated in Fig. 2(a), are analyzed to determine both the charge on the particle and its distribution within

the particle. The final length a is 140 nm for a width b of about 170 nm. Three different regions are distinguished when plotting the measured charge versus the length a of the rectangular contour: Firstly, the enclosed charge increases rapidly, corresponding to contours which sweep across the particle; second there are oscillations as the contours cross the boundary of the particle, and, finally, the signal plateaus out in the vacuum. The latter region is most easily interpreted: the total measured charge remains constant within the contours since the vacuum contains no charge. The total charge on the particle can be determined from the average in this region as $49.7 \pm 3q_e$. Note that the error was estimated by taking into account correlations due to the finite resolution of the phase image (see the Supplemental Material [26], Suppl. C).

In order to quantify which charge sensitivity is achieved with a single contour integral we created a statistic of independent contours with a defined enclosed area and computed their standard deviations (assuming equal enclosed charges). The result shown in Fig. 3 reveals the enclosed area (or contour integral resolution) required to measure a charge integrated from a certain density with certain precision [e.g., a single contour enclosing 800 nm^2 within particle 1 would contain approximately $6.8q_e$ measured with confidence 68% (1σ)]. That indicates that the small error of the determined total charge on particle 1 stems from the large statistic of contour integrals in vacuum.

In order to explore the limits of the method, we have analyzed a smaller particle ($16 \times 23 \times 28$ nm) which was in electrical contact with the carbon support [Fig. 4(a)].

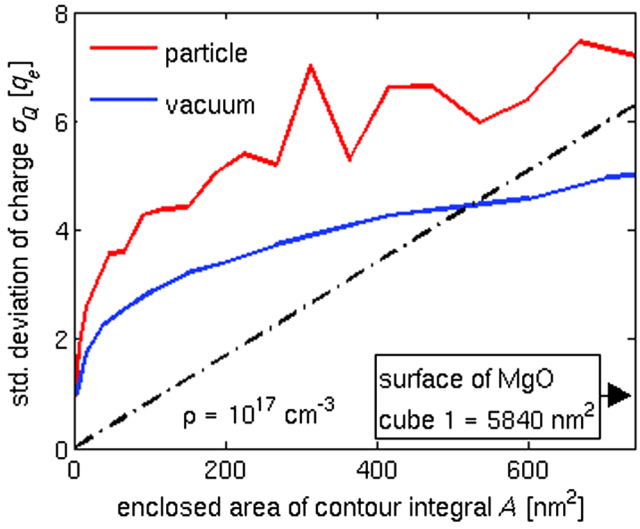

FIG. 3 (color online). Charge error versus spatial resolution: standard deviation of enclosed charge as function of enclosed area within particle 1 (red) and vacuum (blue). The dashed line indicates the enclosed charge assuming a homogeneous projected charge density $\rho = 8 \times 10^{11}$ cm^{-2} as measured for particle 1. The threefold amplification of the standard deviations within the particle corresponds well to the increased phase noise resulting from lower contrast and intensity within the particle [28].

Here, the total charge was $Q = 24.2 \pm 1.2q_e$, measured from the contours extending into the vacuum [Fig. 4(b)]. The increase of charges within the particle follows again a linear slope. We also analyzed a set of contours which start just inside the particle [dotted line in Fig. 4(b)]. We found that the total measured charge was only $Q = 5.1 \pm 1.2q_e$, which demonstrates that very small numbers of charges can be detected with this method.

In both cases, the first part of the curves fit well with a linear slope suggesting a homogeneous distribution of projected charge within the particles. By extending the linear slopes to the particle edge and comparing the intersection with the measured total charge one furthermore observes a discrepancy. For instance, this difference

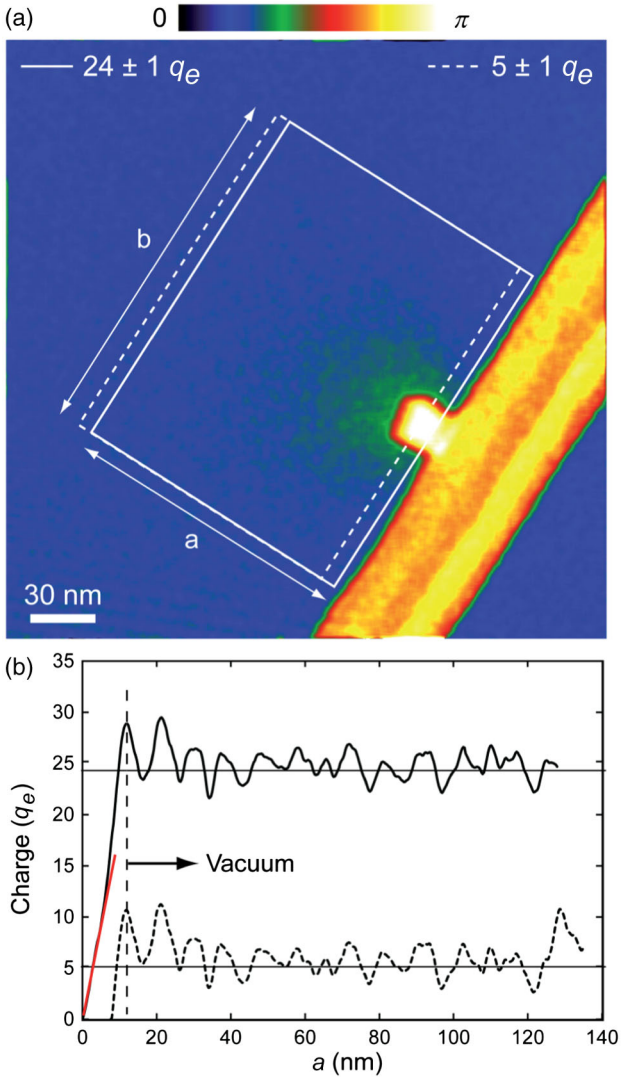

FIG. 4 (color online). Charge measurements on a small particle: (a) reconstructed phase image of particle 2; (b) by contour enclosed charge as a function of the short side a. The full (dotted) line corresponds to the straight (dotted) contour. The linear fit of contours within the particle and the constant fit outside of the particle are indicated by red and black lines, respectively.

is about $10q_e$ for particle 1 [Fig. 2(b)]. That difference indicates the presence of a surface charge. Indeed, assuming a homogeneous distribution of the charges solely on the surface of the cube and knowing the sizes of this particle ($75 \times 78 \times 80$ nm), we can determine using the linear slope ($0.542q_e \cdot \mathrm{nm}^{-1}$) a surface charge of about $1.7510^{-3}q_e \cdot \mathrm{nm}^{-2}$ and a total charge on the lateral face (75×80 nm^2) of $10.5q_e$. That agrees with the observed $10q_e$ within the measurement error which indicates that the total charge is predominantly distributed over the surface. This result could be explained by surface states or adsorbates acting as charge traps. Note, furthermore, that we always measured a positive total charge for all studied particles (Figs. 2 and 3, and the Supplemental Material [26]).

In total, we have shown that contour integral evaluation in holographic phase images facilitates charge measurement with a precision down to one elementary charge. Our statistical analysis showed how the achievable charge precision is linked to the area and number of contour integrals used; i.e., the above noted precision of one q_e is based on evaluating $O(100)$ contours enclosing $O(10^4$ nm$^2)$. Thus, choosing appropriate contours is the key point to investigate charge distribution at the nanometer scale. The future challenge will be to increase the limited holographic contrast V and total image intensity I which both determine the phase noise $\sigma_\phi^2 \approx I^{-1}V^{-2}$ [29]. To that end higher brightness guns and less smearing detectors are highly useful. At the date of that article such equipment is already available and we are therefore confident that the detection of isolated electrons and detailed charge mapping will be possible in the near future.

The authors acknowledge financial support from the European Union under the Seventh Framework Program under a contract for an Integrated Infrastructure Initiative (Reference 312483-ESTEEM2). G. P. acknowledges the CNRS for supporting him for a 4 month visit at CEMES-CNRS Toulouse.

*Corresponding author.
gatel@cemes.fr

[1] M. J. Yoo, T. A. Fulton, H. F. Hess, R. L. Willett, L. N. Dunkleberger, R. J. Chichester, L. N. Pfeiffer, and K. W. West, Science **276**, 579 (1997).
[2] S. H. Tessmer, P. I. Glicofridis, R. C. Ashoori, L. S. Levitov, and M. R. Melloch, Nature (London) **392**, 51 (1998).
[3] L. Cockins, Y. Miyahara, S. D. Bennet, A. A. Clerk, S. Studenikin, P. Poole, A. Sachrajda, and P. Grutter, Proc. Natl. Acad. Sci. U.S.A. **107**, 9496 (2010).
[4] C. Schönenberger and S. F. Alvarado, Phys. Rev. Lett. **65**, 3162 (1990).
[5] M. T. Woodside and P. L. McEuen, Science **296**, 1098 (2002).
[6] J. Komrska, in *Advances in Electronics and Electron Physics*, edited by L. Marton (Academic, New York, 1971), Vol. 30, p. 139.
[7] J. W. Chen, G. Matteucci, A. Migliori, G. F. Missiroli, E. Nichelatti, G. Pozzi, and M. Vanzi, Phys. Rev. A **40**, 3136 (1989).
[8] D. Cherns and C. G. Jiao, Phys. Rev. Lett. **87**, 205504 (2001).
[9] S. Chung, R. A. Berechman, M. R. McCartney, and M. Skowronski, J. Appl. Phys. **109**, 034906 (2011).
[10] P. F. Fazzini, P. G. Merli, G. Pozzi, and F. Ubaldi, Phys. Rev. B **72**, 085312 (2005).
[11] K. H. Downing, M. R. McCartney, and R. M. Glaeser, Microsc. Microanal. **10**, 783 (2004).
[12] W. D. Rau, P. Schwander, F. H. Baumann, W. Höppner, and A. Ourmazd, Phys. Rev. Lett. **82**, 2614 (1999).
[13] A. C. Twitchett, R. E. Dunin-Borkowski, and P. A. Midgley, Phys. Rev. Lett. **88**, 238302 (2002).
[14] M. R. McCartney, J. Electron Microsc. **54**, 239 (2005).
[15] R. M. Glaeser and K. H. Downing, Microsc. Microanal. **10**, 790 (2004).
[16] T. Kasama, R. E. Dunin-Borkowski, S. B. Newcomb, and M. R. McCartney, Microsc. Microanal. **10**, 988 (2004).
[17] F. Ubaldi, G. Pozzi, T. Kasama, M. R. McCartney, S. B. Newcomb, and R. E. Dunin-Borkowski, J. Phys. Conf. Ser. **209**, 012064 (2010).
[18] G. Matteucci, G. Missiroli, E. Nichelatti, A. Migliori, M. Vanzi, and G. Pozzi, J. Appl. Phys. **69**, 1835 (1991).
[19] G. Matteucci, G. F. Missiroli, and G. Pozzi, Adv. Imaging Electron Phys. **122**, 173 (2002).
[20] T. Latychevskaia, P. Formanek, C. Koch, and A. Lubk, Ultramicroscopy **110**, 472 (2010).
[21] M. Beleggia, T. Kasama, R. E. Dunin-Borkowski, S. Hofmann, and G. Pozzi, Appl. Phys. Lett. **98**, 243101 (2011).
[22] A. Tonomura, Jpn. J. Appl. Phys. **47**, 11 (2008).
[23] A. Lubk, D. Wolf, and H. Lichte, Ultramicroscopy **110**, 438 (2010).
[24] M. Beleggia, T. Kasama, and R. E. Dunin-Borkowski, Ultramicroscopy **110**, 425 (2010).
[25] H. A. Bethe, Ann. Phys. (Berlin) **87**, 55 (1928).
[26] See Supplemental Material at http://link.aps.org/supplemental/10.1103/PhysRevLett.111.025501 for details of the off-axis holography method (Suppl. A), influence of aberrations (Suppl. B), line integral evaluation and error analysis (Suppl. C).
[27] M. Gajdardziska-Josifovska, M. R. McCartney, W. J. Ruijter, D. J. Smith, J. K. Weiss, and J.-M. Zuo, Ultramicroscopy **50**, 285 (1993).
[28] J. Cowley, *Electron Diffraction Techniques* (Oxford University Press, Oxford, 1992), Vol. 1.
[29] F. Lenz, Optik (Stuttgart) **79**, 13 (1988).